Speech Transmission Using Rate-Compatible Trellis Codes and Embedded Source Coding

Alexis Bernard, *Student Member, IEEE,* Xueting Liu, *Member, IEEE,* Richard D. Wesel, *Senior Member, IEEE,* and Abeer Alwan, *Senior Member, IEEE*

***Abstract*—This paper presents bandwidth-efficient speech transmission systems using rate-compatible channel coders and variable bitrate embedded source coders. Rate-compatible punctured convolutional codes (RCPC) are often used to provide unequal error protection (UEP) via progressive bit puncturing. RCPC codes are well suited for constellations for which Euclidean and Hamming distances are equivalent (BPSK and 4-PSK). This paper introduces rate-compatible punctured trellis codes (RCPT) where rate compatibility and UEP are provided via progressive puncturing of symbols in a trellis. RCPT codes constitute a special class of codes designed to maximize residual Euclidean distances (RED) after symbol puncturing. They can be designed for any constellation, allowing for higher throughput than when restricted to using 4-PSK. We apply RCPC and RCPT to two embedded source coders: a perceptual subband coder and the ITU embedded ADPCM G.727 standard. Different operating modes with distinct source/channel bit allocation and UEP are defined. Each mode is optimal for a certain range of AWGN channel SNRs. Performance results using an 8-PSK constellation clearly illustrate the wide range of channel conditions at which the adaptive scheme using RCPT can operate. For an 8-PSK constellation, RCPT codes are compared to RCPC with bit interleaved coded modulation codes (RCPC-BICM). We also compare performance to RCPC codes used with a 4-PSK constellation.**

***Index Terms*—Adaptive multirate (AMR), bit interleaved coded modulation (BICM), embedded coding, punctured codes, rate-compatible channel coding, perceptual coding, rate-compatible punctured convolutional codes (RCPC), rate-compatible punctured trellis codes (RCPT), trellis codes, unequal error protection.**

I. Introduction

In SPEECH communication systems, a major challenge is to design a system that provides good speech quality over a wide range of channel conditions. For rate-constrained systems, one solution consists of allowing the transceivers to monitor the state of the communication channel and to dynamically allocate the bitstream between source and channel coders accordingly. For low signal-to-noise ratio (SNR) channels, the source coder operates at low bit rates, thus allowing powerful forward error control. For high SNR channels, the source coder uses its highest rate resulting in high speech quality. An adaptive algorithm selects the best source-channel coding combination out of a collection of available source and channel coders operating at different rates based on estimates of channel quality.

Channel coders whose redundancy is allowed to vary, thereby adapting the coding rate after the transmitter acquires information about channel conditions, are called variable-rate channel coders. Rate-compatible coders, for which the bit or symbol stream of the channel encoder operating at low redundancy is embedded in the bit or symbol stream of the channel encoder operating at high redundancy, form one class of variable-rate channel encoders.

Speech coders whose operating bit rate is allowed to vary, thereby adapting the rate to channel conditions, are called adaptive multirate (AMR) speech coders (e.g., [1]–[5]). Embedded source coders, for which the bitstream of the source encoder operating at low bit rates is embedded in the bitstream of the coder operating at higher rates, form one class of AMR source encoders.

In this paper, we combine embedded AMR source coding and rate-compatible channel coding to design codecs which make maximum use of the available channel bandwidth using bit prioritized embedded source coders and a new type of rate-compatible channel encoders.

Rate-compatible channel codes, such as Hagenauer's rate-compatible punctured convolutional codes (RCPC) [6], are a collection of codes providing a family of channel coding rates. By puncturing bits in the bitstream, the channel coding rate of RCPC codes can be varied instantaneously, providing unequal error protection (UEP) by imparting on different segments different degrees of protection. Cox *et al.* [7] illustrate how RCPC codes can be used to build a speech transmission scheme for mobile radio channels. Their approach is based on a subband coder with dynamic bit allocation proportional to the average energy of the bands. RCPC codes are then used to provide UEP. A scheme combining multirate embedded source and channel coding to provide speech transmission over an extended range of channel conditions was also described in [8], [9].

We present a novel UEP channel encoding scheme by analyzing how puncturing of symbols in a trellis and the rate-compatibility constraint (progressive puncturing pattern)

Paper approved by A. Goldsmith, the Editor for Wireless Communication of the IEEE Communications Society. Manuscript received July 7, 2000; revised March 15, 2001. This work was supported in part by a subcontract from the NSF-USC ERC, NSF CAREER AWARD NCR-9733089, and Rockwell Semiconductor Systems (now Conexant), Broadcom, and HRL through California Micro program. This paper was presented in part at the 32nd Asilomar Conference on Signals, Sytems and Computers, Monterey, CA, November 1–4, 1998 and at the IEEE International Conference on Acoustics, Speech, and Signal Processing, Phoenix, AZ, March 15–19, 1999.

A. Bernard, R. D. Wesel, and A. Alwan are with the Electrical Engineering Department, University of California, Los Angeles (UCLA), Los Angeles, CA 90095 USA (e-mail: abernard@icsl.ucla.edu; wesel@ee.ucla.edu; alwan@ee.ucla.edu).

X. Liu was with the Electrical Engineering Department, University of California, Los Angeles (UCLA), Los Angeles, CA 90095 USA. She is now with Globespan, Santa Clara, Santa Clara, CA 95051 USA (e-mail: xueliu@globespan.net).

Publisher Item Identifier S 0090-6778(02)01359-4.

0090–6778/02$17.00 © 2002 IEEE

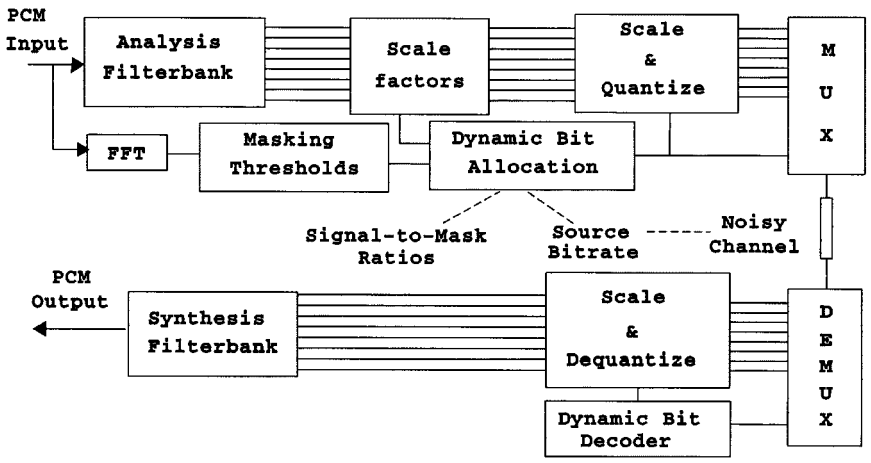

Fig. 1. Block diagram of the perceptually based encoder and decoder.

can be used to derive rate-compatible punctured trellis codes (RCPT). While conceptually similar to RCPC codes, RCPT codes are specifically designed to operate efficiently on large constellations (for which Euclidean and Hamming distances are no longer equivalent) by maximizing the residual Euclidean distance after symbol puncturing. Large constellation sizes, in turn, lead to higher throughput and spectral efficiency on high SNR channels.

Multirate speech coding is not new. Techniques like voice activity detection (VAD) or entropy-matching coding are proposed to decrease average coding bit rates. However, few AMR systems describing both source and channel coding have been presented. Some AMR systems [2]–[5] that combine different types of variable rate CELP coders for source coding with RCPC and cyclic redundancy check (CRC) codes for channel coding were presented as candidates for the European Telecommunications Standards Institute (ETSI) GSM AMR codec standard. In [10], UEP is applied to perceptually based audio coders (PAC). The bitstream of the PAC is divided into two classes and punctured convolutional codes are used to provide different levels of protection, assuming a BPSK constellation.

We design AMR systems based on a perceptually-based embedded subband encoder and the embedded ADPCM standard G.727. Since perceptually based dynamic bit allocation leads to a wide range of bit error sensitivities, the channel protection requirements are determined accordingly. The AMR systems utilize the new rate-compatible channel coding technique (RCPT) for UEP and operate on an 8-PSK constellation. For the same constellation sizes and transmission rates, RCPT codes are compared to RCPC used with bit interleaved coded modulation codes (RCPC-BICM) [11], [12]. We also compare RCPT to RCPC used with 4-PSK. The complete AMR-UEP systems developed for both source coders are bandwidth efficient, operate over a wide range of channel conditions and degrade gracefully with decreasing channel quality. The overall scheme presents a tool for switching (as frequently as every 20 ms) from one rate to another depending on channel conditions. The channel is considered to be AWGN with fixed SNR for the time span of one speech frame (20 ms).

The remainder of this paper is organized as follows. Section II describes the perceptually based and embedded subband coder and analyzes its bit error sensitivities against transmission errors. Section III introduces rate-compatible punctured trellis codes (RCPT) as a new tool for providing efficient rate-compatible unequal error protection with large constellation sizes. A code design strategy for RCPT is given and its performance in comparison with RCPC and RCPC-BICM codes is presented. Section IV presents the design of an AMR source-channel coding scheme for the subband coder of Section II. Section V describes a similar AMR transmission system for the embedded ADPCM standard, G.727.

II. Perceptually Based and Embedded Subband Coder

A. Description of the Coder

The embedded subband coder shown in Fig. 1 is a modified version of the coder presented by Tang *et al.* in [13]. The speech is first divided into 20-ms frames. An IIR QMF filterbank divides each frame into eight subbands that are then individually encoded. For each frame, dynamic bit allocation according to the perceptual importance of each subband is performed. The MPEG psychoacoustic model [14] estimates the signal-to-noise ratio (SNR) required in each band to mask the quantization noise. The dynamic bit allocation (which is the side-information of the coder and is transmitted with the coded bits) translates the SNR prescribed by the model into a bit assignment to scalar quantize the subband samples.

Dynamic bit allocation based on the perceptual characteristics of the signal has two advantages: it minimizes audible distortion by shaping the quantization noise with respect to the speech spectrum, and it allows the same coder to operate at different bitrates. In the case of the subband coder, dynamic bit allocation is progressive and allocates bits of high perceptual importance first and the ones with the least perceptual importance last. This provides a tool for bit prioritization, necessary for UEP.

Fig. 2 shows an example of progressive bit allocation for the case of a coder operating at 32 kb/s for a 4-kHz bandwidth speech signal. Each frame is composed of 160 samples, divided into 8 subbands with 20 samples per subband. Each block shown in Fig. 2 represents the allocation of one bit to all 20 samples in a subband (1 block $=$ 1 kb/s). The first 3 blocks (3 kb/s) are

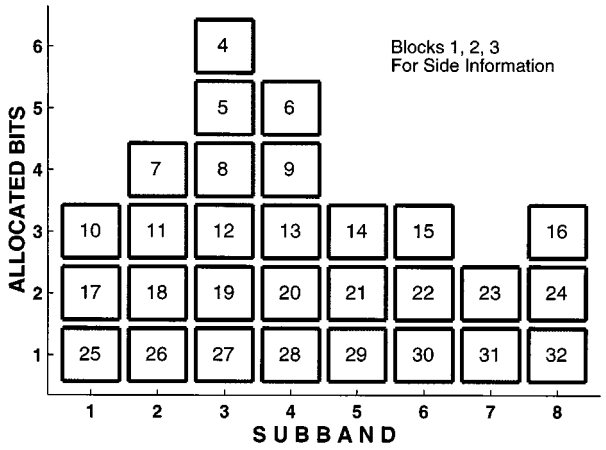

Fig. 2. Example of bit allocation and bit prioritization for the subband coder operating at 32 kb/s. Each block represents the allocation of one bit to each subband sample (1 kb/s). The first three blocks (3 kb/s) are reserved for the transmission of the side information (bit allocation and the different gains). The priority of each block is indicated by the number in its center. Note that the coder operating at m kb/s would consist of the first m allocated blocks.

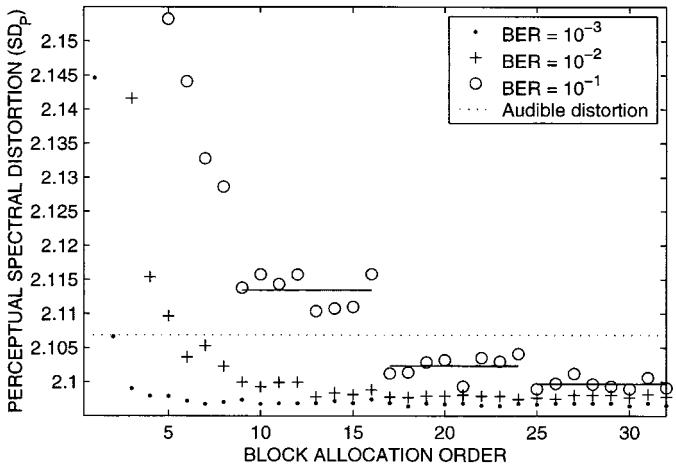

Fig. 3. Bit error sensitivity analysis of the perceptually based subband coder operating at 32 kb/s. Note that sensitivities tend to reach plateaus of eight blocks which typically correspond, for the source coder operating at this rate, to the allocation of one block to each subband. Eight English sentences were used to generate these plots.

dedicated to the transmission of the bit allocation (3 bits/band), the frame gain (4 bits) and the bands' gains (4 bits/band), for a total of 60 bits per frame. The allocated bitstream is prioritized using 20-bit segments, selecting the blocks in Fig. 2 from top to bottom and from left to right. The allocation order of each block is indicated by the number in its center. The coder, robust against acoustic noise, offers embedded variable bitrate source coding with reasonable to excellent speech quality in the range 8–32 kb/s.

B. Bit Error Sensitivities of the Perceptual Subband Coder

In Section III, we will show how rate-compatible punctured trellis codes can be used in order to provide UEP. For this purpose, we derive the maximum BER tolerable for each bit in the bitstream below which the effect of channel errors is inaudible.

The notion of determining the relative importance of bits for further UEP was pioneered by Rydbeck and Sundberg [15], [16]. One can define the bit error sensitivity (BES) of a given bit in the bitstream as the relative increase in speech distortion due to transmission errors at that particular bit position. Typically, BES is computed by measuring the segmental SNR after setting bits in errors [15].

In the perceptually based subband coding scheme, the signal-to-mask ratio (SMR) of each subband is computed. The SMR indicates the perceptual importance of each band. We refine the BES analysis by computing the increase in speech distortion due to setting bits in error at different BERs using a distortion metric that takes into account the masking properties of auditory perception. The perceptual spectral distortion (SD_P) measure between the original spectrum $A(f)$ and the reconstructed spectrum $\hat{A}(f)$ is defined as follows:

$$\mathrm{SD}_p(\hat{A}(f), A(f)) = \sqrt{\sum_{i=1}^{N} \mathrm{SMR}(i) \int_{f=f_i^l}^{f=f_i^u} 10 \log \frac{|\hat{A}(f)|^2}{|A(f)|^2}\, df}$$

where N is the number of bands and f_i^l, f_i^u, and $\mathrm{SMR}(i)$ represent the lower frequency, the upper frequency, and the weighting function, respectively, for the ith subband. $\mathrm{SMR}(i)$ is defined as $\mathrm{SMR}(i) = \max_{f \in [f_i^l, f_i^u]} \mathrm{SMR}(f)$.

Fig. 3 illustrates the BES for the coder operating at its maximum rate, i.e., 32 kb/s. The sensitivity of each block against channel errors is computed by averaging the BES of the 20 bits in that block. Individual BES are simulated by systematically setting for each frame the particular bit position in error with a probability of error equal to the BER of interest and keeping all other bit positions error-free. Speech material used consists of eight English sentences (four male and four female talkers) from the TIMIT [17] database. The dotted horizontal line represents the maximum tolerable distortion due to channel errors. At this distortion level, informal listening tests indicated that speech distortion introduced by channel impairment is practically transparent to the listener, in the sense that an increment in distortion due to channel transmission is indistinguishable from the distortion introduced by the source coder.

Fig. 3 shows that the sensitivity to transmission errors of the first three blocks is very high even for $\mathrm{BER} = 10^{-3}$, and may be beyond scale for larger BERs. Those blocks correspond to the side information (bit allocation and bands gains) and forward error correcting codes should assure that they are sufficiently protected. A second observation is that at this rate, the last bits in the bitstream are relatively insensitive to channel errors. Even with a BER as high as 10^{-1}, distortion is below the sensitivity threshold. These bits barely need protection against channel impairment. Finally, observe that the almost monotically decreasing nature of Fig. 3 justifies *a posteriori* the perceptual and dynamic bit allocation algorithm.

III. Rate-Compatible Punctured Trellis Codes

Rate-compatible channel codes provide a method for unequal error protection. One of the main advantages of rate-compatible convolutional or trellis codes is that they allow the use of the same decoding structure for multiple code rates, since the decoding trellis remains unchanged through puncturing.

Punctured convolutional codes were introduced in [18], mainly as a lower complexity alternative to high rate convolutional coding. Hagenauer added the rate-compatibility restriction to derive the concept of RCPC codes as a special case of punctured convolutional codes [6]. For convolutional codes, it has been shown that rate-compatible codes can be as good as the best known conventional codes of the same constraint length [6]. Symbol-wise periodic puncturing of trellis codes introduced in [19], [20] provides an alternative to bit puncturing. If progressive symbol puncturing is required, rate-compatible punctured trellis codes (RCPT) are obtained.

The effect of periodically puncturing bits or symbols is to remove periodic subsequences of bits (before signal mapping) or constellation points, respectively, before transmission. As the number of punctured bits or symbols increases, the information rate per transmitted symbol increases and the BER performance of the code degrades. With rate-compatible puncturing codes, all codes, except the one with the lowest rate, are derived by puncturing bits from the convolutional coder (RCPC) or symbols from the trellis coder (RCPT) with the lowest rate.

In [21] and [6], Lee and Hagenauer present convolutional codes and rate-compatible puncturing patterns leading to good RCPC codes. Below we discuss the design of a trellis code and the selection of progressive puncturing patterns defining efficient RCPT codes.

With RCPT, a puncturing pattern that removes q symbols out of every p symbols (p is the puncturing period) is a $p-q$ puncturing pattern. The average per-symbol information rate R associated with a $p-q$ puncturing pattern applied to a rate k/n code and a 2^n constellation size is given by

$$R = \frac{pk}{p-q} \tag{1}$$

where $0 \leq q < p$.

In a sequence of progressive puncturing patterns, let $\tilde{a}^q$, a vector of p binary elements, be a pattern with q punctured symbols. A "1" in $\tilde{a}^q$ means that the symbol is transmitted and a "0" means that the symbol is not transmitted (punctured). To provide rate-compatibility, once a symbol is punctured at a given rate, it must also be punctured at any higher rate, i.e., $\tilde{a}^{q+1}$ can only be formed by replacing one remaining "1" of $\tilde{a}^q$ with a "0". Note that in order to avoid negative redundancy ($R > n$), one must satisfy $q \leq \lfloor p(1-k/n) \rfloor$.

The trellis used in the soft Viterbi decoding of the received symbols has the same structure throughout all of the puncturing patterns. Puncturing any symbol before transmission can be represented in the receiver by setting all branch metrics associated with the corresponding nonreceived symbol to zero. The same decoder can be used with all coding rates, and the rate can change during decoding, as with RCPC.

A. RCPT Code Design

RCPT codes are a particular case of the symbol-punctured trellis codes for periodic erasures introduced in [19], [20]. For RCPT codes, the puncturing vector $\tilde{a}^q$ must also satisfy the condition for rate-compatibility, i.e., progressive puncturing.

The periodic distance vector for trellis codes is first defined. Let the normalized symbol-wise squared Euclidean distance between the ith symbols of two trellis events be $d_i^2(x \to \hat{x}) = (x_i - \hat{x}_i)^2/\varepsilon_x$, where x_i and $\hat{x}_i$ are the correct and incorrect constellation points associated with the ith symbols of a trellis error event, respectively, and ε_x is the average constellation energy. The periodic puncturing of symbols scales the distances with the same index modulo p by the binary scale factor $\tilde{a}_i$. Define the periodic squared distance $\tilde{d}_i^2$ for any given index i and puncturing period p as the sum of the square of the distances scaled by the same factor a_i,

$$\tilde{d}_i^2(x \to \hat{x}) = \sum_{m=0}^{\infty} d_{i+mp}^2. \tag{2}$$

The p values of $\tilde{d}^2 = [\tilde{d}_1^2 \cdots \tilde{d}_p^2]$ form the periodic distance vector.

The usual optimality criterion for minimizing the BER for trellis codes under AWGN is a large free Euclidean distance. The minimum Euclidean distance remaining after puncturing q symbols out of every p symbols ($p-q$ puncturing) using the puncturing pattern $\tilde{a}^q$ is referred to as the residual Euclidean distance RED_q, and is computed as an inner product:

$$\mathrm{RED}_q(\tilde{a}(q)) = \min_{\tilde{d}^2} \langle \tilde{a}(q)^2, \tilde{d}^2 \rangle. \tag{3}$$

Note that if two output sequences after puncturing are identical, the RED is zero. Note also that when designing a trellis code for periodic symbol puncturing, the necessary condition for rate-compatibility limits the number of puncturing families $\{\tilde{a}\}$ to consider, where $\{\tilde{a}\}$ is the set of all puncturing families.

In practice, finding the best code and puncturing patterns to minimize the BER under different puncturing patterns would require extensive simulations, or at least a union bounding. However, asymptotic coding gains for trellis codes are linear in the minimum Euclidean distance of the code expressed in dB. Thus, RED is a good (but not exact) indicator of BER under puncturing.

RCPT code design is a multi-criterion problem since we have to minimize the BER (maximize RED) at all rates (puncturing patterns) simultaneously. The best performance for a particular puncturing level will often be obtained at the expense of suboptimal performance for another puncturing level. We refer to a trellis code as undominated if no trellis codes of the same complexity performs better on every channel in the family. Typically, there will be several undominated trellis codes. Such undominated solutions are called Pareto optimal. To select among the Pareto optimal codes, we chose equal weighting of asymptotic coding gains as a sensible way to resolve the multi-criterion problem. The design criterion is thus the maximization over all Pareto-optimal codes of J_{dB}, the logarithmic sum of all RED values of interest,

$$J_{\mathrm{dB}} = \sum_{q=0}^{\lfloor p(1-\frac{k}{n}) \rfloor} 10 \log_{10}(\mathrm{RED}_q). \tag{4}$$

The limits of the summation represent the puncturing patterns of interest, which range from no puncturing $q=0$, to puncturing all redundancy added by the channel encoder $q = p(1-k/n)$. We emphasize that other reasonable approaches exist to choose

TABLE I
CHARACTERISTICS OF THE 8-PSK, 16-STATES ($\nu = 4$), RATE-$1/3$ AND PERIOD-8 RCPT CODES

RCPT Generator Matrix = [32 11 27] $\nu = 4$, $p = 8$ symbols, rate = $1/3$			
q	**Rate**	**Puncturing**	$\mathbf{RED}_q^2$
0	1.000	11111111	12.60
1	1.142	01111111	8.34
2	1.333	01110111	6.34
3	1.600	01010111	4.58
4	2.000	01010101	4.58
5	2.667	00010101	1.17

TABLE II
CHARACTERISTICS OF THE 16-QAM, 64-STATES ($\nu = 6$), RATE-$1/4$ AND PERIOD-8 RCPT CODES

RCPT Generator Matrix = [43 175 155 103] $\nu = 6$, $p = 8$ symbols, rate = $1/4$			
q	**Rate**	**Puncturing**	$\mathbf{RED}_q^2$
0	1.000	11111111	12.4
1	1.142	01111111	8
2	1.333	01110111	7.6
3	1.600	01010111	4.8
4	2.000	01010101	4.4
5	2.667	00010101	1.2

a final code from the set of Pareto optimal codes. This objective function gives equal weight to the asymptotic SNR requirements of each puncturing pattern. We ran an exhaustive search with this objective function to find the best candidate over all Pareto optimal codes and progressive puncturing families.

The Viterbi decoding complexity of a trellis code depends both on the number of memory elements ν (number of states is $S = 2^{\nu}$), and on the traceback depth L_D of the decoding process. For standard trellis or convolutional codes, L_D is computed as the trellis depth at which all unmerged error events have more Euclidean distance than the minimum Euclidean distance of the trellis code [22]. The traceback depth for a specific puncturing pattern dropping q symbols, written $(L_D)_q$, is the trellis depth at which all unmerged incorrect paths exceed the residual Euclidean distance RED_q.

Catastrophic behavior occurs when an infinite number of bit errors result from a finite Euclidean distance error event, i.e., the encoder state diagram has a loop that has zero output Hamming weight and nonzero input Hamming weight. Even if the original encoder is not catastrophic, periodic puncturing of symbols may lead to catastrophic behavior. A technique for determining catastrophic behavior under periodic symbol erasures is presented in [20], [23]. Our search used this technique to rule out combinations of codes and puncturing families that were catastrophic at any rate of interest. Recently, a more efficient technique for identifying catastrophic behavior was presented in [24].

Whether or not codes generally exist using our design procedure depends on whether codes exist that can be maximally punctured without becoming catastrophic. We do not have proof of the existence of such codes, but we have examined several scenarios and never found a case where such codes did not exist. As an example, a rate-$1/3$ RCPT code designed for an 8-PSK constellation with puncturing period $p = 8$ symbols and with 4 memory elements ($\nu = 4$ or 16 states) was found using the J_{dB} criterion and is presented in Table I. The generator matrices are given in octal notation (e.g., 43 stands for $1+D+D^5$). Euclidean distances throughout these results assume a two-dimensional constellation with a unit average energy. As expected, RED typically decreases as more symbols are punctured, increasing the information rate.

Another example of RCPT code, designed for a 16-QAM constellation, is shown in Table II. It is a rate-$1/4$, 64-state and period-8 code. For the curve with information rate of 1 bit per symbol, [19] shows that there is a penalty of about 1 dB at $\mathrm{BER} = 10^{-5}$ between the RCPT code and the best known code with information rate of 1 bit per symbol (the feedforward rate-$1/2$ maximum Hamming distance convolutional code $[G = 131\ 171]$ used with Gray-labeled 4-PSK). However, [20] shows another example of a 64-state, period-5, rate-$1/3$ RCPT code used on an 8-PSK constellation $[G = 171\ 46\ 133]$ where for the same information rate of one bit per symbol, there is no penalty associated with the rate compatibility constraint.

In general, punctured trellis codes are competitive with standalone codes for information rates of 1 and 2 bits per symbol while providing greater rate flexibility. For relatively high target BER, appropriate for speech transmission, the punctured codes are also competitive at three information bits per symbol.

As observed in [19] and more carefully examined in [20], the determining factor for the loss imposed on trellis code performance by a rate-compatibility constraint is constellation size. Specifically, for a rate of K bits per symbol, if the constellation is significantly larger than 2^{K+1} points, as with a 16-QAM constellation for $K = 1$, the rate-compatible code will have some performance loss as compared to a single-rate code using a 2^{K+1}-point constellation and a standard set-partitioning code. Note that the larger constellation is required for the rate-compatible code to support higher information rates. An 8-PSK constellation represents a good tradeoff, giving a relatively wide range of rates with negligible performance loss from a set-partitioning code at $K = 1$.

For any periodic puncturing vector and channel noise variance, periodic transfer function bounds producing asymptotically tight bounds on BER can also be computed [20]. However, we used simulation results to obtain the low-SNR BER performance necessary for our system design.

B. Comparison of Rate-Compatible Codes

Table III compares 64-state RCPT, RCPC-BICM, and RCPC codes by providing the information rate per symbol R, the puncturing vector $\tilde{a}^q$, the residual squared Euclidean distances RED^2, the traceback depth (L_D), and the number of nearest neighbors (N) for different puncturing levels. The nearest number is computed as the sum of the number of minimum Euclidean distances error events starting at each phase normalized by the number of phases (i.e., the period p). The left panel of Table III presents a 64-state, rate-$1/3$, 8-PSK RCPT code with period $p = 9$, describing performance and decoding complexity at each puncturing pattern in its family. Note that RCPT codes

TABLE III
CHARACTERISTICS OF THE 8-PSK 64-STATE ($\nu = 6$) RATE-$1/3$ RCPT AND RCPC-BICM CODES, AND THE 4-PSK 64-STATE ($\nu = 6$) RATE-$1/2$ RCPC CODES

RCPT Rate = 1/3 8-PSK constellation G = [165 142 127] p = 9 symbols					
ID	Rate	Puncturing Vector	RED^2	L_D	N
a	1.00	111111111	16	24	1
b	1.12	111111110	11.2	25	0.22
c	1.29	111101110	9.17	26	0.44
d	1.50	110101110	6.93	31	0.33
e	1.80	110101100	4.34	31	0.66
f	2.25	100101100	1.76	27	0.22
g	3.00	100101000	0.59	36	1
8	3.00	Uncoded 8-PSK	0.59	0	2

RCPC-BICM Rate = 1/3 8-PSK constellation G = [155 127 117] p = 3 × 9 bits					
ID	Rate	Puncturing Matrix	RED^2	L_D	N
A	1.00	111111111 111111111 111111111	8.79	21	3
B	1.12	111111111 111101111 111101101	7.03	22	0.22
C	1.29	111101101 111101101 111101101	5.86	21	0.33
D	1.50	101101101 101101101 101101101	5.86	28	11.1
E	1.80	101101001 101101001 101101001	4.10	34	2.33
F	2.25	101001001 001101001 101001001	2.34	45	0.22
–	3.00	Catastr.			
8	3.00	Uncoded 8-PSK	0.59	0	2

RCPC Rate = 1/2 4-PSK constellation G = [133 171] p = 2 × 8 bits					
ID	Rate	Puncturing Matrix	RED^2	L_D	N
A	1.00	11111111 11111111	20	27	11
B	1.14	11111111 11101110	14	27	0.5
C	1.33	11111111 10101010	12	34	0.5
D	1.60	11111111 10001000	8	48	0.75
E	1.78	11110111 10001000	6	92	0.5
–	2.00	Catastr.			
4	2.00	Uncoded 4-PSK	1	0	2

are able to operate after all redundancy has been removed (case g) with the same free Euclidean distance as uncoded transmission, but it does not perform as well as uncoded 8-PSK modulation in simulation. This means that if there are no channel errors, the decoder is capable of recovering exactly the original bit sequence since the non zero RED after extreme puncturing is sufficient to distinguish different trellis events.

For comparison, the right panel of Table III also summarizes the performance of 64-state RCPC codes [6]. Since RCPC codes are designed especially for Hamming distances, we use the 4-PSK constellation and consider rate-$1/2$ convolutional codes. The RCPC system consistently provides a slightly better Euclidean distance at a slightly higher information rate as compared to RCPT for its rate family. However, this Euclidean distance advantage appears negligible in simulations at the BERs of interest, apparently because the RCPT code has a smaller number of nearest neighbors. Furthermore, the Euclidean distance advantage of RCPC is small compared to the disadvantage of the rate limitation at high SNR imposed by the 4-PSK constellation as compared to the 8-PSK constellation used for RCPT.

We also consider bit interleaved coded modulation (BICM) codes [11], [12] that can use Hamming-distance-based convolutional codes with any constellation. In order to use RCPC with an 8-PSK constellation, we modify BICM in such a way as to make the coder rate-compatible using progressive puncturing of bits after convolutional encoding. The resulting coder is a rate compatible punctured bit interleaved convolutional coder, referred to as RCPC-BICM. The middle panel of Table III shows performance of a 64-state RCPC-BICM with a rate-$1/3$ convolutional encoder, a puncturing period of $p = 3 \times 9$ bits and an 8-PSK constellation. The information rates are the same as for those for the RCPT codes. RCPT generally provides a better Euclidean distance than RCPC-BICM. The residual Euclidean distance for RCPC-BICM is computed from the residual Hamming distance (RHD) of the convolutional encoder after puncturing as follows:

$$\mathrm{RED}_q^2 = \mathrm{RHD}_q \cdot (2\sin(\pi/8))^2. \tag{5}$$

Raw BER versus SNR curves of the RCPT, RCPC-BICM and RCPC codes with six memory elements for a standard AWGN channel are presented in Fig. 4. However, in the design of AMR transmission systems, we are concerned with how much source coding information can be transmitted using the different coding schemes depending on the BER requirements and the channel SNR. Fig. 5 illustrates the different achievable information rates (source bits/transmitted symbols) as a function of the AWGN channel SNR, assuming that a BER of 10^{-3} is required. Note that the curves with rates equal to 2 and 3 are obtained using uncoded 4- and 8-PSK, respectively. Two observations are made: 1) RCPT and RCPC-BICM operate at the same rates, but RCPT outperforms since transitions to larger information rates occur at lower SNRs; 2) despite RCPCs better free Euclidean distances, RCPT and RCPC behave similarly at low SNRs. RCPT benefits at high SNR from its larger constellation size and exhibits larger information rates. Although Fig. 5 considers only $\mathrm{BER} = 10^{-3}$, similar behavior is observed at different BERs. In summary, RCPT offers a wider efficient operating range than RCPC since it is specifically designed for a larger constellation, permitting larger throughput. In addition, RCPT combines coding and modulation, allowing for improved performance with respect to RCPC-BICM.

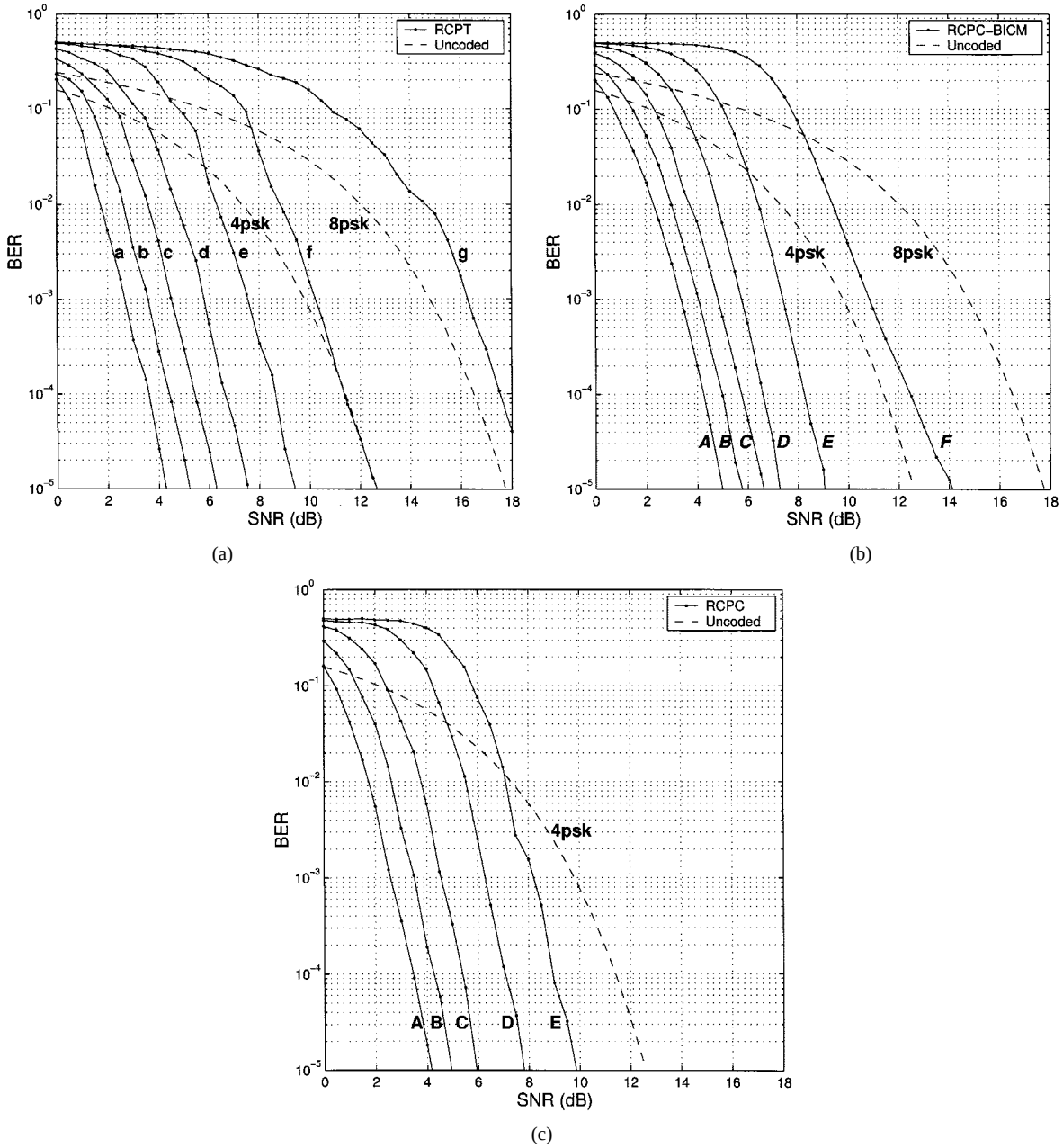

Fig. 4. BER curves for the (a) RCPT, (b) RCPC-BICM, and (c) RCPC encoding schemes presented in Table III over an AWGN channel. Traceback depth used is 41.

Note that for Rayleigh fading channels, RCPC-BICM codes would be superior since the residual diversity after puncturing would be equal to RHD. However, this assumes ideal interleaving, which in turn requires interleaver depths of at least the coherence time of the channel. This might not be tolerable for speech coding applications where the overall transmission delay must be kept at a minimum.

C. Traceback Depth and Frame Size

It is interesting to study the effect of the frame size on the transition between RCPT code rates within a frame. Fig. 6 illustrates the three levels of protection offered by the $c, d,$ and e curves of the RCPT code of Table I operating on an AWGN channel at 7 dB and their corresponding information rate per symbol R. Each code rate is used for 96 bits, which corresponds to twice the longest traceback depth. Note that the effect of the traceback depth in the trellis is visible at transition zones. When transitioning from a p–q puncturing to a p–$(q+1)$ puncturing, branch metrics degrade and performance starts degrading $(L_D)_q$ bits before the transition (i.e., as soon as the Viterbi decoder must trace back through symbols with increased puncturing). State metrics (or path metrics) explain the behavior of the BER versus bit position curve after switching. The superior quality of the state metrics at the end of the $p-q$ puncturing pattern enhances performance at the beginning of the $p-(q+1)$ puncturing pattern, and it takes approximately another $(L_D)_{q+1}$ symbols for the quality of these path metrics to fully degrade to the steady quality of the $p-(q+1)$ pattern. The transition zone length is then approximately $(L_D)_q + (L_D)_{q+1}$ symbols.

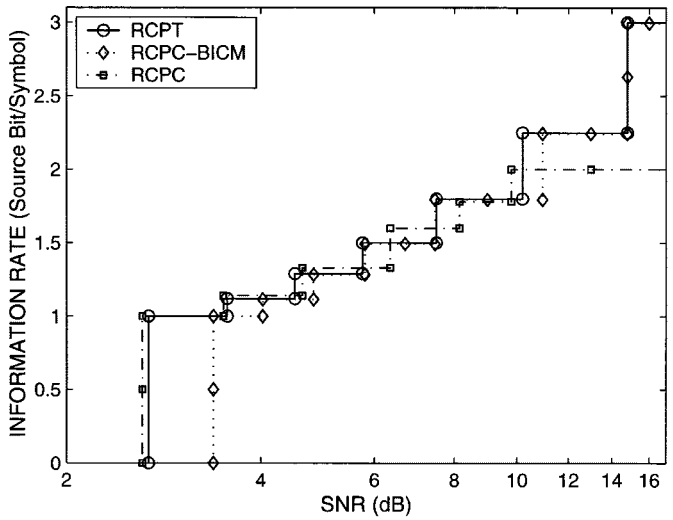

Fig. 5. For a required BER level of 10^{-3} and an AWGN channel, the figure illustrates the achievable information rates (in source bits/transmitted symbols) for RCPT, RCPC-BICM, and RCPC as a function of the channel SNR. The information rates and SNR for 10^{-3} can also be found in Fig. 4.

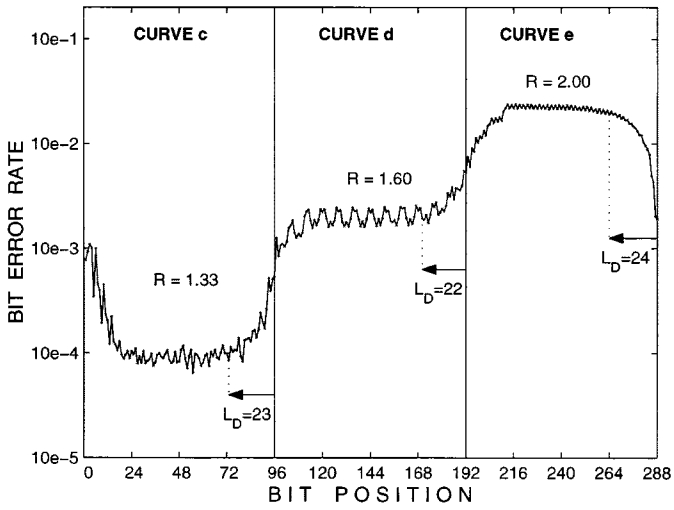

Fig. 6. Unequal error protection illustration using RCPT curves c, d, and e of Table I. The operating channel SNR is 7 dB. The traceback depth used throughout the frame is $L = 48$. Each level of protection is 96 bits long.

In Table III, we see that RCPT codes have smaller traceback depths than RCPC and RCPC-BICM for the most severe puncturings. This means that RCPT codes can usually operate with smaller frame sizes and buffering delays.

IV. AMR System Design for the Subband Coder

We design a source-channel coder system leading to high speech quality over a wide range of channel conditions in three steps. First, for each part of the bitstream and for every SNR, rates of protection needed to obtain BERs that have corresponding inaudible distortions are determined. Second, we determine the maximum source coding bitrate that can satisfy these BER conditions given the average redundancy inferred by the rates of protection required. Finally, the puncturing architecture of the coded bitstream is derived so that the final source-channel coded bitstream equals 20 kb/s for the 4-PSK RCPC or 30 kb/s for both 8-PSK RCPT and RCPC-BICM

TABLE IV
Unequal Error Protection Puncturing Architecture for RCPT, RCPC-BICM, and RCPC Codes of Table III Applied to the Subband Coder. The Notation x_n Indicates That n Bits Are Protected Using the x Curve

Rate [kbps]	bits/ frame	RCPT	RCPC-BICM	RCPC
10	200	a_{200}	A_{200}	A_{200}
12	240	$a_{60}b_{40}c_{140}$	$A_{60}B_{40}C_{140}$	$A_{60}B_{40}C_{140}$
14	280	$b_{60}c_{80}4_{140}$	$B_{60}C_{80}4_{140}$	$B_{60}C_{80}D_{140}$
16	320	$b_{20}c_{60}d_{140}4_{100}$	$B_{20}C_{60}D_{140}4_{100}$	$C_{80}D_{140}E_{40}4_{60}$
18	360	$c_{60}d_{120}4_{120}8_{60}$	$C_{60}D_{120}4_{120}8_{60}$	$D_{80}E_{160}4_{120}$
20	400	$d_{80}e_{340}8_{200}$	$D_{80}E_{340}8_{200}$	4_{400}
22	440	$e_{320}8_{120}$	$E_{320}8_{120}$	
24	480	$e_{200}f_{160}8_{120}$	$E_{200}F_{160}8_{120}$	
26	520	$e_{120}f_{160}8_{240}$	$E_{120}F_{160}8_{240}$	
28	560	$f_{320}8_{240}$	$F_{320}8_{240}$	
30	600	8_{600}	8_{600}	

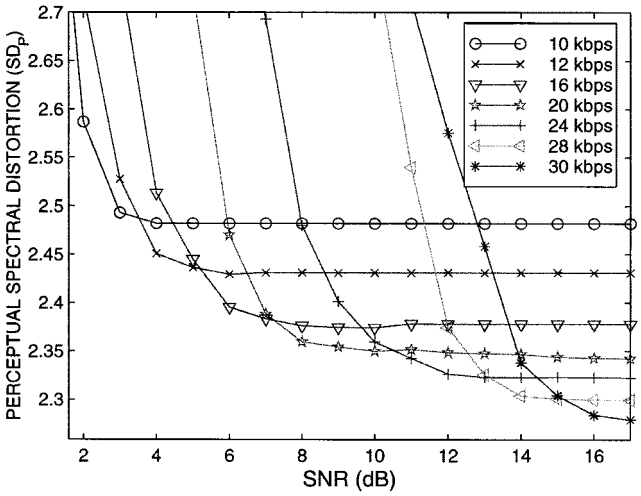

Fig. 7. Perceptual spectral distortion (SD_P) for the subband coder with RCPT at different bit rates over an AWGN channel.

(i.e., 10 kbaud/s for each scheme). Table IV summarizes the puncturing architecture for the channel encoders and for different source coding bitrates, assuming we use the subband coder (Section II) and the RCPT, RCPC-BICM, and RCPC codes given in Table III. In addition to the various puncturing patterns, we make use of both uncoded 4-PSK and 8-PSK curves. In Table IV, the notation a_m, b_n, c_p, indicates that the first m bits in the prioritized bitstream are protected using the puncturing pattern a, the following n bits with the puncturing pattern b and finally the last p bits with the puncturing pattern c. Note also that the number of bits protected with any given level of protection are generally at least twice the traceback depth of the level of protection considered.

Fig. 7 shows the quality of the different source-coder/RCPT-channel-coder pairs simulated with $L_D = 32$ on independent AWGN channels (for clarity, only a few of the source coding bit rates are shown). As expected, no specific source coding rate systematically outperforms the others. At low SNRs the 10-kb/s source coder with full protection outperforms, while at high SNRs, the coders with large source coding bitrates provide the least speech distortion. At every SNR, we select the source-channel system that provides the best speech quality. The overall distortion-SNR curve is the minimum of all the curves

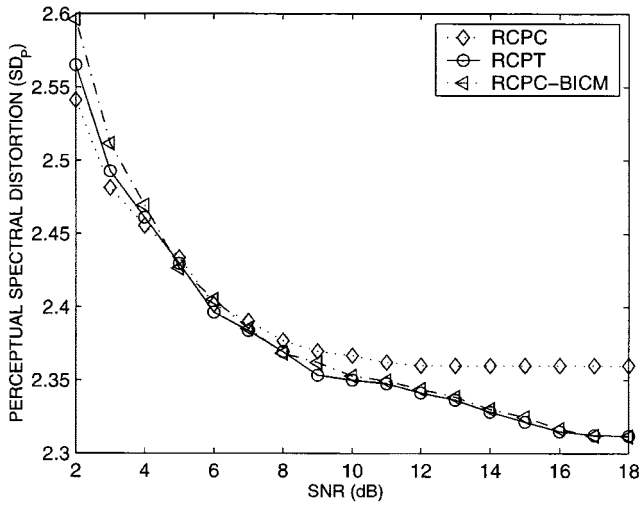

Fig. 8. Comparison of the source-channel coding schemes operating distortion curves (lower envelopes) using RCPC, RCPT, and RCPC-BICM over an AWGN channel.

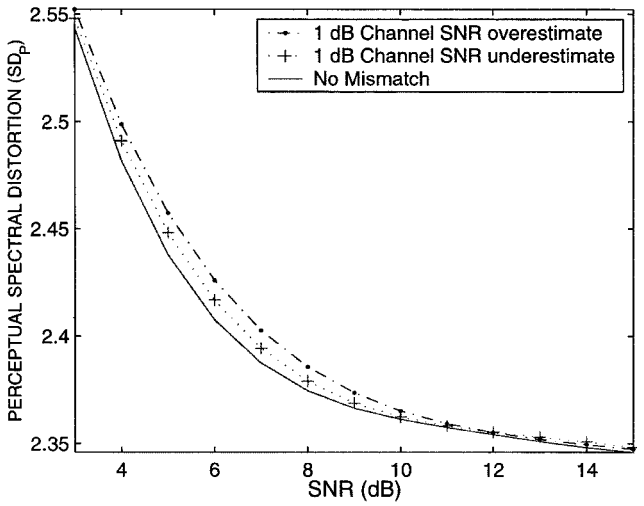

Fig. 9. Effect of channel mismatch on the system performance subband source coder-RCPT channel coder.

at each SNR. This is an operational rate-distortion curve for this system [25], [26].

Fig. 8 compares the minimum perceptual distortion obtained for every SNR using the subband coder with RCPC, RCPT and RCPC-BICM codes over an AWGN channel. For Figs. 7 and 8, speech material used was eight English sentences (four males and four females) from the TIMIT database. For each channel SNR and for each channel coding scheme, the smallest spectral distortions obtained by running the system for all the possible source and channel rates are shown in Fig. 8. Perceptual speech distortion decreases with increasing SNR and is kept limited even at very low SNR; this would not be true for a scheme with fixed source bit rate and no rate-compatible channel encoder. Furthermore, each rate-distortion curve in Fig. 8 is lower than if equal error protection was used. Both results demonstrate that AMR speech transmission systems can provide good speech quality over a wide range of channel conditions.

Note that RCPT and RCPC provide comparable speech quality at intermediate SNRs. However, RCPT produces less distortion at high SNRs, due to its higher per-symbol information rate. Indeed, with a 4-PSK constellation, RCPC allows only up to 20 kb/s joint source-channel bitrates, while the 8-PSK constellation of RCPT and RCPC-BICM permits 30 kb/s overall bitrates. This effect is noticeable only at high SNRs, where the mutual information of an 8-PSK constellation exceeds the maximum mutual information of a 4 PSK constellation. At intermediate SNRs the per-symbol information rates obtained from both coders are similar. Note also that at low SNR, RCPT results in less distortion when compared to RCPC-BICM. In summary, RCPT allows for both larger bit rates at high SNRs, by using large constellations, and good code performance at low SNRs by combining coding and modulation. It should also be stated that the source-channel coding rates combination that minimizes speech distortion for any channel SNR is exactly the one that was specifically designed for that SNR. This justifies *a posteriori* the AMR system design procedure whose criterion, in the tradeoff between source and channel distortions, was to keep channel distortions just below the audibility threshold.

The AMR system works under the assumption that slow channel tracking permits switching to the best AMR operating mode for each channel condition. When channel quality is underestimated, speech quality could be improved by switching to a source coding rate appropriate to the true channel characteristics. When channel quality is overestimated, channel coding protection is not sufficient enough to protect the bitstream against channel errors, resulting in degraded speech quality. Fig. 9 shows the effect of channel mismatch on the AMR system performance. It can be seen that overestimating channel quality leads to an erroneous bitstream whose corresponding speech distortion is higher than when using an underperforming source coder as a result of channel quality underestimation.

V. AMR System Design for the G.727 Embedded ADPCM Coder

In the previous sections, we showed how an embedded and perceptual coder could be coupled with rate-compatible channel coders in order to build a channel-adaptive speech transmission system with UEP. This section shows that rate-compatible channel coding techniques providing UEP are not specific to perceptual coders and can also be applied to other embedded source coding schemes such as the ITU standard G.727 codec [27].

A. Description of the Embedded ADPCM G.727 Coder

Embedded ADPCM algorithms are a family of variable bit rate coding algorithms operating on a sample-by-sample basis that allows for bit dropping after encoding. As with the subband coder, the decision levels of the lower rate quantizers are subsets of those of the quantizers at higher rates. This allows for bit reduction at any point in the network without the need for coordination between the transmitter and the receiver.

Simplified block diagrams of an embedded ADPCM encoder and decoder are shown in Fig. 10. Embedded ADPCM algorithms produce code words that contain enhancement and core bits. The feedforward (FF) path of the codec utilizes both enhancement bits and core bits, while the feedback (FB) path uses

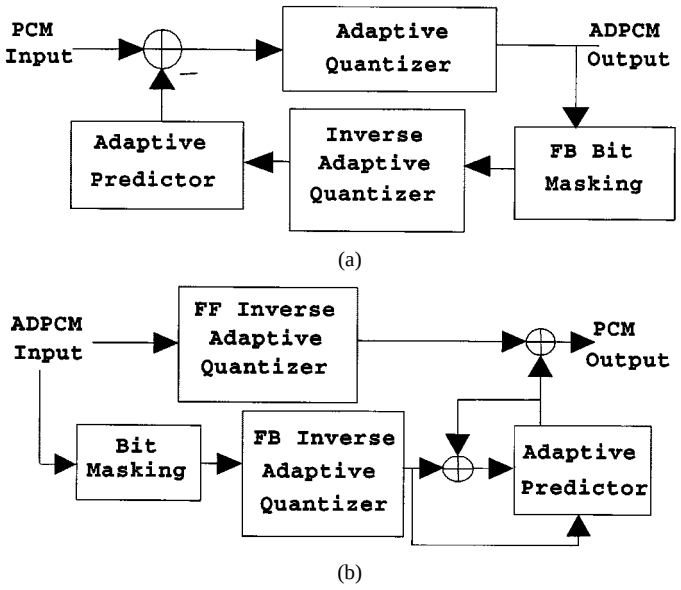

Fig. 10. Simplified diagrams of the embedded ADPCM G.727 codec. (a) Encode. (b) Decoder.

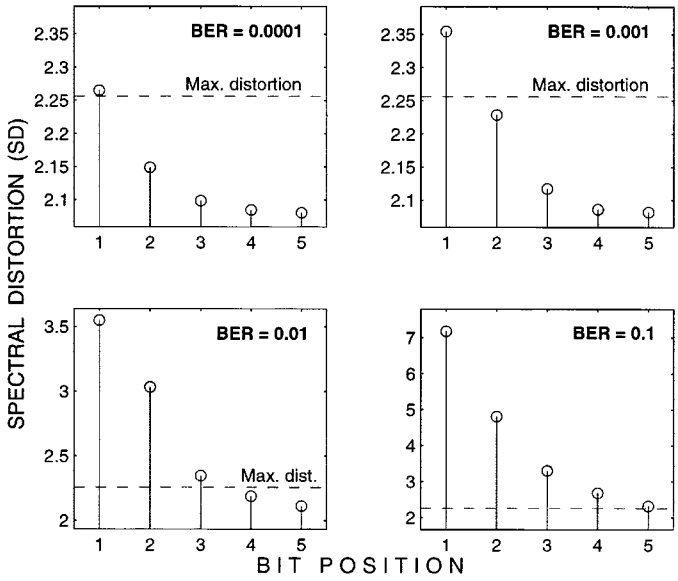

Fig. 11. Bit error sensitivity analysis for embedded ADPCM (5, 2) at 40 kb/s (5 bits/sample).

core bits only. With this structure, enhancement bits can be discarded or dropped during network congestion. Embedded ADPCM algorithms are referred to by (n, m) pairs where n refers to the FF (enhancement and core) bits and m refers to the FB (core) bits. For example, the (5, 2) coder operates at 40 kb/s (5 bits/sample) while the (4, 2), (3, 2), and (2, 2) pairs represent the 32-kb/s, 24-kb/s, and 16-kb/s algorithms, respectively, embedded in the 40 kb/s coder.

B. Bit Error Sensitivity Analysis

ADPCM coders do not provide any SMR information. In this case, we use the spectral distortion metric (SD) introduced in [28]

$$\mathrm{SD}(\hat{A}(f), A(f)) = \sqrt{\frac{1}{W_0}\int |W_B(f)|^2 10\log\frac{|\hat{A}(f)|^2}{|A(f)|^2}\,df}$$

where W_0 is a normalization constant and W_B is a hearing sensitivity weighting function defined by

$$W_B(f) = \frac{1}{25 + 75(1 + 1.4(f/1000)^2)^{0.69}}. \qquad (6)$$

Fig. 11 illustrates the effect of transmission errors on the five different bit positions in a 5 bits/sample ADPCM encoder (5, 2). Also represented in Fig. 11 is the level of distortion for which the incremental distortion introduced by channel impairment is inaudible. This level is obtained by informal listening tests. In the (5, 2) ADPCM encoding pair, the two first bits (FB bits) are fed back into the adaptive predictor, resulting in error propagation. Therefore, their sensitivity to channel inaccuracy is high. The three last bits (FF bits) are less sensitive to transmission errors and tolerate transmission error rates up to around 10^{-2} (in contrast with the perceptual SBC coder at 32 kb/s which could tolerate BERs up to 10^{-1}).

C. AMR System Design for G.727

In order to define the puncturing architecture that provides different levels of protection for bits in the bitstream, we follow the same steps used for designing an AMR system for the subband coder.

However, a major difference between the two coders is that for the subband coder, bits are grouped in frames, while the G.727 coder operates on a sample-by-sample basis. As we have seen in Fig. 5, the traceback depth requirements of the Viterbi decoder requires that we apply the same level of protection to at least as many bits as twice the maximum traceback depth of the code. Therefore, we cannot change the protection requirement on a sample-by-sample basis. For an (n, m) embedded ADPCM encoder, one needs to frame at least $2 \cdot \max(L_D)$ samples together and group them into maximum n groups requiring different sensitivities. The disadvantage of this procedure is the introduction of a buffering delay in the communication link proportional with the traceback depth of the channel code. For instance, using the RCPT code presented in Table III and taking $2 \cdot \max(L_D)$ as the minimum group size, 72 samples must be grouped to form a frame, which corresponds to a minimum buffering delay of 9 ms. If the RCPC code of Table III had been used, at least 184 samples should be grouped, which corresponds to a buffering delay of 23 ms. Note that the buffering delay increases with the mother code complexity and that RCPT codes provide smaller traceback depth requirements than RCPC.

With G.727, the source bitrate varies from 16 kb/s to 40 kb/s in steps of 8 kb/s. For the combined source-channel coding scheme, we limit the source-channel bitrate to 45 kb/s, i.e., the baudrate is 15 ksymbols/s with an 8-PSK constellation for RCPT and RCPC-BICM. For RCPC and its 4-PSK constellation, in order to keep approximately the same baudrate, one limits the overall bit rate to 32 kb/s.

Table V illustrates the puncturing architecture for the $(n, 2)$ ADPCM encoders with $2 \leq n \leq 5$. The subscripts represent

TABLE V
UNEQUAL ERROR PROTECTION PUNCTURING ARCHITECTURE FOR RCPT, RCPC-BICM, AND RCPC CODES OF TABLE III APPLIED ON THE EMBEDDED ADPCM G.727 CODER

ADPCM pair	Bits/ Sample	Rate [kbps]	RCPT	RCPC-BICM	RCPC
(2,2)	2	16	a_1 b_1	A_1 B_1	A_1 B_1
(3,2)	3	24	$c_1 d_1 e_1$	$C_1 D_1 E_1$	$C_1 E_2$
(4,2)	4	32	$d_1 e_1$ $f_1 8_1$	$D_1 E_1$ $F_1 8_1$	8_4
(5,2)	5	40	e_1 $f_1 8_3$	E_1 $F_1 8_3$	

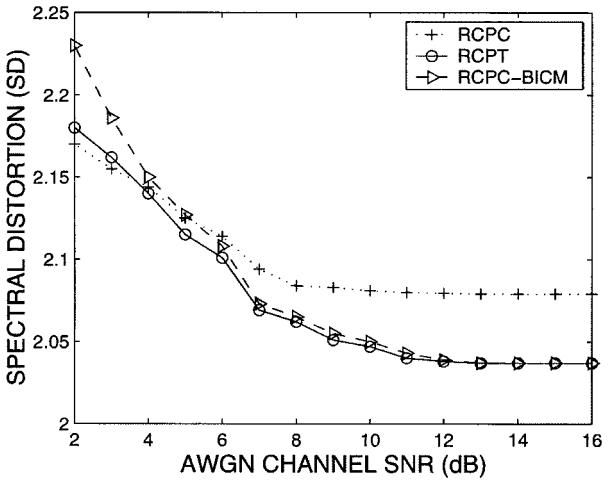

Fig. 12. Operating distortion curves using RCPC, RCPT and RCPC-BICM with the embedded ADPCM coder.

the number of bits per sample protected with the corresponding puncturing level. This number has to be multiplied by the frame size in samples/frame in order to compute the number of successive bits being similarly protected.

Simulations combining RCPT, RCPC-BICM, and RCPC codes with embedded ADPCM at different source coding rates are performed. Again, according to channel conditions, one can select the mode with the least distortion. The operational distortion-SNR curves of the AMR-UEP systems operating on an AWGN channel are shown in Fig. 12. The operational distortion-SNR curves are monotically decreasing and operate on a wide range of channel conditions. Higher transmission rates allow RCPT and RCPC-BICM to outperform RCPC at high SNRs. At low SNRs, RCPT outperforms RCPC-BICM due to its superior residual Euclidean distance profile.

VI. DISCUSSION AND CONCLUSIONS

We have shown how to combine embedded and variable bit rate speech source encoders with rate-compatible channel codes to build AMR transmission systems and obtain high quality speech over a wide range of channel conditions. Different operating modes can be selected at each time instant according to channel quality. Graceful speech degradation is obtained with decreasing channel SNR. Switching between rates is transparent and can be made frequently. We illustrated the design of AMR systems for both a perceptual subband speech coder and the G.727 speech coder using an 8-PSK constellation.

We introduced the RCPT codes and compared their performance with RCPC and RCPC-BICM codes. RCPT codes are designed to maximize the Euclidean distance between trellis error events whereas RCPC codes maximize Hamming distance. For 4-PSK, RCPC codes also maximize Euclidean distance, but for larger constellations, they are suboptimal. Larger constellation sizes are important for larger throughput. For instance, it would be interesting to propose RCPT codes for upcoming EDGE (enhanced data rate GSM evolution) channels, which will be using 8-PSK constellations. The advantage RCPT has over RCPC-BICM comes from the combination of trellis coding and modulation for an improved Euclidean distance profile. Also, RCPT decoding typically requires a smaller punctured traceback depth than RCPC and RCPC-BICM, hence it requires smaller frame sizes and buffering delays. Finally, by dropping symbols instead of bits, RCPT codes provide variable *baud* rates. This can be useful in situations where it is advantageous to lower the symbol throughput or the transmitter power consumption. The robustness and flexibility of the progressive symbol puncturing scheme make the proposed architecture promising for communication channels where deep fade or strong interference can be modeled as symbol puncturing.

The intrinsic embedded structure of both source and channel encoders offers multiple advantages. First, the entire AMR system can be implemented using a single codec. Only the number of allocated bits and the puncturing table need to be updated at the transmitter when switching between operating modes. At the receiver, adjustment to rate changes is simple. Branch metrics corresponding to the punctured symbols in the Viterbi decoder are set to zero according to the puncturing table.

Second, one can drop bits or symbols anywhere in the transmission link, without having to re-encode the signal. This offers flexibility for traffic management.

Third, embedded source coders usually produce bits with a wide range of predictable sensitivities against channel errors and are therefore well suited for unequal error protection. We have shown, for instance, that perceptually based dynamic bit allocation can isolate several bits in the bitstream that are almost insensitive to channel errors and can be left unprotected. In addition, embedded coding structures allow for multi-resolution coding, which is highly desirable for delay sensitive communication systems, as there is no need to wait for the reception of the entire bitstream before recovering speech of reasonable quality.

Finally, we showed how BES analysis could help determine for each bit position the maximum tolerable BER that keeps channel distortion inaudible from source coding distortion. A technique for finding the optimal puncturing schemes for different channel conditions and source bit rates has also been presented.

Systems using AMR source and channel coding are likely to be integrated in future communication systems. We have provided some examples that demonstrate the potential for RCPT AMR systems to provide graceful speech degradation over a wide range of channel SNR.

REFERENCES

[1] A. Gersho and E. Paksoy, "An overview of variable rate speech coding for cellular networks," in *Proc. IEEE Int. Conf. Select. Topics in Wireless Commun.*, June 1999, pp. 172–175.

[2] J. Vainio, H. Mikkola, K. Jarvinen, and P. Haavisto, "GSM EFR based multi-rate codec family," in *Proc. ICASSP 1998*, vol. 1, May 1998, pp. 141–144.
[3] A. Uvliden, S. Bruhn, and R. Hagen, "Adaptive multi-rate. A speech service adapted to cellular radio network quality," in *Proc. 32nd Asilomar Conf. Signals, Systems and Computers*, vol. 1, Nov. 1998, pp. 343–347.
[4] E. Paksoy, J. C. de Martin, A. McCree, C. Gerlach, A. Anandakumar, M. Lai, and V. Viswanathan, "An adaptive multi-rate speech coder for digital cellular telephony," in *Proc. ICASSP 1999*, vol. 1, 1999, pp. 193–196.
[5] H. Ito, M. Serizawa, K. Ozawa, and T. Nomura, "An adaptive multi-rate speech codec based on MP-CELP coding algorithm for ETSI AMR standard," in *Proc. ICASSP 1998*, vol. 1, Apr. 1998, pp. 137–140.
[6] J. Hagenauer, "Rate-compatible punctured convolutional codes and their applications," *IEEE Trans. Commun.*, vol. 36, pp. 389–400, Apr. 1988.
[7] R. Cox, J. Hagenauer, N. Seshadri, and C.-E. Sundberg, "Subband speech coding and matched convolutional channel coding for mobile radio channels," *IEEE Trans. Signal Processing*, vol. 39, pp. 1717–1731, Aug. 1991.
[8] D. J. Goodman and C. E. Sundberg, "Combined source and channel coding for variable bit-rate speech transmission," *Bell Syst. Tech. J.*, vol. 62, pp. 2017–2036, Sept. 1983.
[9] ——, "Transmission errors and forward error correction in embedded differential PCM," *Bell Syst. Tech. J.*, vol. 62, pp. 2735–2764, Nov. 1983.
[10] D. Sinha and C.-E. Sundberg, "Unequal error protection methods for perceptual audio coders," in *Proc. ICASSP 1999*, vol. 5, Mar. 1999, pp. 2423–2426.
[11] G. Caire, G. Taricco, and E. Biglieri, "Bit-interleaved coded modulation," *IEEE Trans. Inform. Theory*, vol. 44, pp. 927–946, May 1998.
[12] E. Zehavi, "8-PSK trellis codes for a Rayleigh channel," *IEEE Trans. Commun.*, vol. 40, pp. 873–884, May 1992.
[13] B. Tang, A. Shen, A. Alwan, and G. Pottie, "A Perceptually-based embedded sub-band speech coder," *IEEE Trans. Speech Audio Processing*, vol. 5, no. 2, pp. 131–140, Mar. 1997.
[14] K. Brandenburg and G. Stoll, "ISO-MPEG-1 audio: A generic standard for coding of high quality digital audio," *J. Audio Eng. Soc.*, vol. 42, no. 10, pp. 780–792, Oct. 1994.
[15] N. Rydbeck and C. E. Sundberg, "Analysis of digital errors in nonlinear PCM systems," *IEEE Trans. Commun.*, vol. COM-24, pp. 59–65, Jan. 1976.
[16] C. E. Sundberg, "The effect of single bit errors in standard nonlinear PCM systems," *IEEE Trans. Commun.*, vol. COM-24, pp. 1062–1064, June 1976.
[17] V. Zue, S. Seneff, and J. Glass, "Speech database development at MIT: TIMIT and beyond," *Speech Commun.*, vol. 9, no. 6, pp. 351–356, Aug. 1990.
[18] J. B. Cain, G. C. Clark, and J. M. Geist, "Punctured convolutional code off rate $(n-1)/n$ and simplified maximum likelihood decoding," *IEEE Trans. Inform. Theory*, vol. 20, pp. 388–389, May 1974.
[19] R. D. Wesel, X. Liu, and W. Shi, "Periodic symbol puncturing of trellis codes," in *Proc. 31st Asilomar Conf. Signals, Systems and Computers*, vol. 1, Nov. 1997, pp. 172–176.
[20] ——, "Trellis codes for periodic erasures," *IEEE Trans. Commun.*, vol. 48, pp. 938–947, June 2000.
[21] L. H. C. Lee, "New rate-compatible punctured convolutional codes for Viterbi decoding," *IEEE Trans. Commun.*, vol. 41, pp. 3073–3079, Dec. 1994.
[22] J. B. Anderson and K. Balachandran, "Decision depths of convolutional codes," *IEEE Trans. Inform. Theory*, vol. 35, pp. 455–459, Mar. 1989.
[23] R. D. Wesel and X. Liu, "Analytic techniques for periodic trellis codes," in *Proc. 36th Allerton Conf. Commun., Contr., Computing*, Sept. 1998, pp. 39–48.
[24] C. Fragouli, C. Kominakis, and R. D. Wesel, "Minimality under periodic puncturing," in *Proc. ICC*, vol. 1, June 2001, pp. 300–304.
[25] A. Bernard, X. Liu, R. Wesel, and A. Alwan, "Channel adaptive joint-source channel coding of speech," in *Proc. 32nd Asilomar Conf. Signals, Systems Computers*, vol. 1, Nov. 1998, pp. 357–361.
[26] ——, "Embedded joint-source channel coding of speech using symbol puncturing of trellis codes," in *Proc. ICASSP 1999*, vol. 5, Mar. 1999, pp. 2427–2430.
[27] *5, 4, 3 and 2 Bits Samples Embedded Adaptive Differential Pulse Code Modulation (ADPCM)*, 1990. ITU, Recommendation G.727.
[28] A. McCree, K. Truong, E. B. George, T. P. Harnwell, and V. Viswanathan, "A 2.4 kbps MELP coder candidate for the new U.S. Federal Standard," in *Proc. ICASSP 1996*, vol. 1, Apr. 1996, pp. 200–203.

Alexis Bernard (S'97) was born in Brussels, Belgium, in 1973. He received the B.S. degree from the Université Catholique de Louvain (UCL), Louvain-La-Neuve, Belgium, and the M.S. degree from the University of California, Los Angeles (UCLA), in 1998, both in electrical engineering. He is currently pursuing the Ph.D. degree in electrical engineering at UCLA.

During 1994–1995, he was an exchange scholar at the Katholieke Universiteit Leuven (KUL), Belgium. He has worked as an intern for several companies, including Alcatel Telecom, Antwerp, Belgium (1997), and Texas Instruments, Dallas (1999 and 2000). His current research interests include the design of source and channel coding methods for speech coding and speech recognition.

Mr. Bernard is a recipient of the Belgian American Educational Foundation Fellowship.

Xueting Liu (S'00–M'01) received the B.S. degree in automatic control engineering from Central South University of Technology, Changsha, China, in 1992, the M.S. degree from the Institute of Automation, Chinese Academy of Sciences, Beijing, in 1995, and the Ph.D. degree in electrical engineering from University of California, Los Angeles (UCLA), in 2000.

She is currently with Globespan, Santa Clara, CA. Her research interests include the design of robust and adaptive trellis codes and joint source channel coding.

Richard D. Wesel (S'91–M'96–SM'01) was born in Marietta, OH, in 1966. He received the S.B. and S.M. degrees in electrical engineering from the Massachusetts Institute of Technology, Cambridge, both in 1989, and the Ph.D. degree in electrical engineering from Stanford University, Stanford, CA, in 1996.

From 1989 to 1991 he was a Member of Technical Staff with AT&T Bell Laboratories. His work at AT&T resulted in two patents. Since 1996 he has been with the University of California, Los Angeles (UCLA) as an Assistant Professor with the Electrical Engineering Department. His research interests are in the area of communication theory with particular interest in the topics of channel coding and distributed communication.

Dr. Wesel has received a National Science Foundation CAREER Award, an Okawa Foundation award, and the TRW Excellence in Teaching Award from the UCLA Henry Samueli School of Engineering and Applied Science. He has been an Associate Editor for the IEEE TRANSACTIONS ON COMMUNICATIONS in the area of coding and communication theory since 1999.

Abeer Alwan (S'82–M'85–SM'00) received the Ph.D. degree in electrical engineering from the Massachusetts Institute of Technology, Cambridge, in 1992.

Since then, she has been with the Electrical Engineering Department, University of California, Los Angeles (UCLA) as an Assistant Professor (1992–1996), Associate Professor (1996–2000), and Professor (2000–present). She established and directs the Speech Processing and Auditory Perception Laboratory at UCLA. Her research interests include modeling human speech production and perception mechanisms and applying these models to speech-processing applications such as automatic recognition, compression, and synthesis. She is an Editor-in-Chief of *Speech Communication*.

Dr. Alwan is a member of Eta Kappa Nu, Sigma Xi, Tau Beta Pi, the New York Academy of Sciences, and the IEEE Signal Processing Technical Committees on Audio and Electroacoustics and on Speech Processing. She served, as an elected member, on the Acoustical Society of America Technical Committee on Speech Communication from 1993 to 1999. She is the recipient of the NSF Research Initiation Award (1993), the NIH FIRST Career Development Award (1994), the UCLA-TRW Excellence in Teaching Award (1994), the NSF Career Development Award (1995), and the Okawa Foundation Award in Telecommunications (1997).